Research article

Inki Kim[a], Sunae So[a], Ahsan Sarwar Rana, Muhammad Qasim Mehmood and Junsuk Rho*

Thermally robust ring-shaped chromium perfect absorber of visible light

https://doi.org/10.1515/nanoph-2018-0095
Received July 12, 2018; revised August 27, 2018; accepted September 23, 2018

Abstract: A number of light-absorbing devices based on plasmonic materials have been reported, and their device efficiencies (or absorption) are high enough to be used in real-life applications. Many light-absorbing applications such as thermophotovoltaics and energy-harvesting and energy-sensing devices usually require high-temperature durability; unfortunately, noble metals used for plasmonics are vulnerable to heat. As an alternative, refractory plasmonics has been introduced using refractory metals such as tungsten (3422°C) and transition metal nitrides such as titanium nitride (2930°C). However, some of these materials are not easy to handle for device fabrications owing to their ultra-high melting point. Here, we propose a light absorber based on chromium (Cr), which is heat tolerant due to its high melting temperature (1907°C) and is compatible with fabrication using conventional semiconductor manufacturing processes. The fabricated device has >95% average absorption of visible light (500–800 nm) independent of polarization states. To verify its tolerance of heat, the absorber was also characterized after annealing at 600°C. Because of its compactness, broadband operational wavelength, and heat tolerance, this Cr perfect absorber will have applications in high-temperature photonic devices such as solar thermophotovoltaics.

Keywords: refractory materials; solar thermophotovoltaics; plasmonic resonance; impedance matching with free space.

1 Introduction

Optical metamaterials composed of deep subwavelength unit-cell arrays provide a new way to use carefully designed nanostructures to control light. Light-matter interaction at the nanoscale can dramatically improve or adjust the absorption, refraction, and propagation of light. Especially, ultra-thin photonic devices based on 2D optical metamaterials have been used to realize flat optical components [1–5], optical cloaking devices [6], and holograms [7–10]. Perfect light-absorbing devices [11–15] have possible solar energy applications such as solar thermophotovoltaics (STPV).

Most of the metamaterial perfect absorbers are based on plasmonic materials such as gold (Au) [16], silver (Ag) [17], nickel [18], and aluminum [19]. These materials are strongly lossy in visible wavelengths, and by adjusting their nanostructure geometries, their resonance wavelength can be tuned to maximize light absorption.

STPV often works at very high temperatures [20–22], which can damage most plasmonic materials. Bulk noble metals used in plasmonics, such as Ag (961.8°C), Au (1064°C), and palladium (1555°C), have high melting temperature T_M, but their nanostructures deform at far lower temperature than T_M; accordingly, their optical properties can change [23]. As an alternative, several refractory materials have been suggested for heat-tolerant perfect absorbers. Those refractory materials have high melting temperature and exhibit highly lossy dielectric-like properties. For instance, perfect absorbers based on tungsten or titanium nitride (TiN) [24–27] have been demonstrated theoretically and experimentally. Tungsten and TiN have high T_M; this trait makes them heat tolerant but complicates the manufacture of devices based on them. Moreover, most of them are easily oxidized or chemically unstable. For example, TiN has T_M of 2977°C, but at temperature above 800°C it readily oxidizes and loses its plasmonic properties [28].

[a]**Inki Kim and Sunae So:** These authors contributed equally to this work.
***Corresponding author: Junsuk Rho,** Department of Mechanical Engineering, Pohang University of Science and Technology (POSTECH), Pohang 37673, Republic of Korea; Department of Chemical Engineering, Pohang University of Science and Technology (POSTECH), Pohang 37673, Republic of Korea; and National Institute of Nanomaterials Technology (NINT), Pohang 37673, Republic of Korea, e-mail: jsrho@postech.ac.kr.
http://orcid.org/0000-0002-2179-2890
Inki Kim and Sunae So: Department of Mechanical Engineering, Pohang University of Science and Technology (POSTECH), Pohang 37673, Republic of Korea
Ahsan Sarwar Rana and Muhammad Qasim Mehmood: Department of Electrical Engineering, Information Technology University of the Punjab, Lahore 54000, Pakistan

To overcome these limitations of refractory materials, protection layers have been proposed [29, 30]. Chemically [31] and thermally stable thin dielectric layers can be applied in plasmonics system, and this strategy opens a new way to render photonic devices chemically and thermally robust. Plasmonic systems coated with protection layers show stable optical characteristics under intense laser illumination and high-temperature annealing [29, 30].

Here, we demonstrate a chromium (Cr)-based ultrathin, broadband, and heat-tolerant perfect absorber of visible light. Cr metal has high T_M of 1907°C and is inexpensive and easy to fabricate using conventional semiconductor manufacturing processes. We use a 4-nm-thick alumina protection layer to increase the heat tolerance and then confirm its absorbing characteristics. The fabricated device had >95% average absorption of visible light (wavelengths $500 \le \lambda \le 800$ nm) independent of polarization state; this trait was not affected when the device was annealed at 600°C. We also perform full-wave electromagnetic simulation to identify the light-absorbing mechanism.

2 Results and discussion

2.1 Cr metamaterial absorber design

The Cr metamaterial absorber (Figure 1A) is composed of a top layer of ring-shaped Cr nanostructures, an SiO_2 spacing layer, and a bottom perfectly reflecting Cr layer. The whole device thickness is 250 nm (top layer, 40 nm; middle layer, 60 nm; bottom layer, 150 nm) and is fabricated on a silicon substrate to assess the possibility of incorporating the device in a photonic chip or silicon-based electrical or photonic components. The total area of the device is 100×100 μm (Figure 1B). The symmetrical ring-shaped Cr nanostructure is designed to achieve polarization independence at normal incidence. Thus, under unpolarized light, Cr light absorbers can maintain their absorbing effectiveness. Cr can also be easily deposited and patterned using electron beam evaporation and electron beam lithography processes. Nanoimprint lithography or roll-to-roll imprinting methods could be used to fabricate the Cr absorbers over a much larger area.

The Cr absorber was simulated (Figure 1C) in the visible regime using the finite element method on a commercial software (COMSOL). The device showed 98.0% average absorption at $500 \le \lambda \le 800$ nm and >99% absorption at 600 nm $\le \lambda \le 710$ nm. The refractive index of Cr was taken from the CRC Handbook of Chemistry and Physics [32].

Fabricated devices were characterized using Fourier transform infrared (FT-IR) spectroscopy. In FT-IR, the sample is illuminated with unpolarized light at a normal incident angle (Figure 1A). The measurements confirmed that the fabricated device absorbed 95.6% of visible light at $500 \le \lambda \le 800$ nm (Figure 1C). The slight discrepancy between simulated and measured spectra is a result of fabrication errors.

The absorption mechanism of the Cr ring absorber can be ascribed to a combination of plasmonic resonances and impedance matching with free space. The material properties of Cr match the impedance matching of free space at visible wavelengths and also have the plasmonic effect and thereby field localization [33]. Furthermore, the ring-shaped structure allows better impedance matching with free space compared to that of disk-shaped structure, so reflectance is weak and absorbance is strong over the broadband region. To understand the absorption

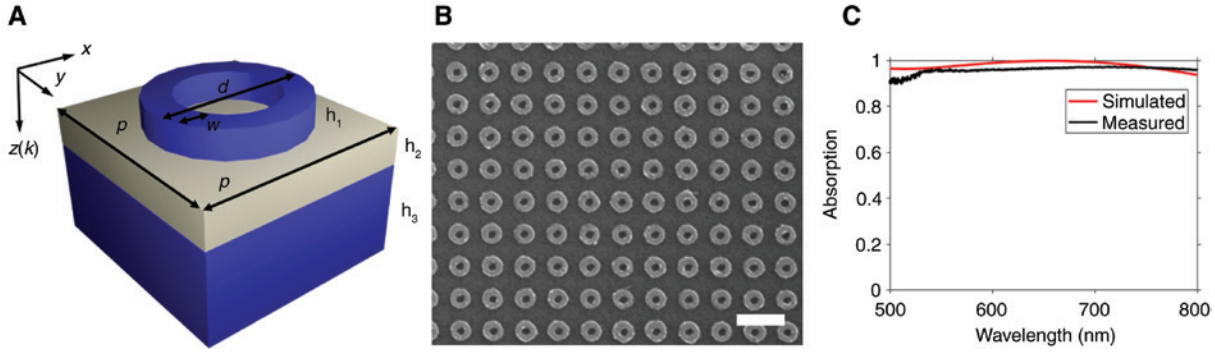

Figure 1: Cr absorbers.
(A) Schematic of Cr absorber unit cell with dimensions of $p = 300$ nm, $w = 40$ nm, $d = 160$ nm, $h_1 = 40$ nm, $h_2 = 60$ nm, and $h_3 = 150$ nm. Blue, Cr; gray, silica. (B) Scanning electron microscopy (SEM) image of the fabricated device. Scale bar, 500 nm. (C) Simulated and measured absorption spectra.

mechanism analytically, we calculated the absorption contribution of each Cr layer (Figure 2A). In each Cr layer, the total power dissipation density Q_{abs} was calculated for the absorbed electromagnetic power as

$$Q_{abs} = \langle J \cdot E \rangle = \sigma |E|^2 = \frac{1}{2}\varepsilon_0 \varepsilon_r'' \omega |E|^2 \quad (1)$$

where σ is the electrical conductivity, ε_0 is permittivity of the vacuum, ε_r'' is the imaginary part of the relative permittivity of the material, ω is angular frequency, and $|E|^2$ is the amplitude of the total electric field within the material. The retrieved structural impedance has two peaks (Figure 2B), which cause the resonant peaks in Figure 2A. The impedance of the device was obtained assuming that the devices are homogenous using the *S*-parameter retrieval method [34]:

$$z = \pm\sqrt{\frac{(1+S_{11})^2 - S_{21}^2}{(1-S_{11})^2 - S_{21}^2}} \quad (2)$$

To further explore the two resonances, we also analyzed normalized surface plots of electric and field distribution (Figure 2C) and normalized magnetic field (Figure 2D) at wavelengths $\lambda_1 = 421$ nm and $\lambda_2 = 564$ nm on the xy- and xz-planes. At $\lambda_1 = 421$ nm, magnetic field distribution clearly shows the magnetic dipolar resonance that occurs because of the coupling between the two Cr layers, in which antiparallel current density J_d creates a loop and thereby an artificial magnetic dipole moment. At $\lambda_2 = 564$ nm, the electric field shows electric dipolar resonance at the top ring antenna. Therefore, our absorber excites electric and magnetic resonances at each corresponding wavelength to increase the localized electromagnetic field.

We also determined whether the absorbance of the device was affected by light angular and polarization. Owing to the symmetrical geometry of the ring antenna, our device absorbs broadband light regardless of polarization at normal incidence (Figure 3A and B). However, at incident angle $\theta_I > 60°$, absorption

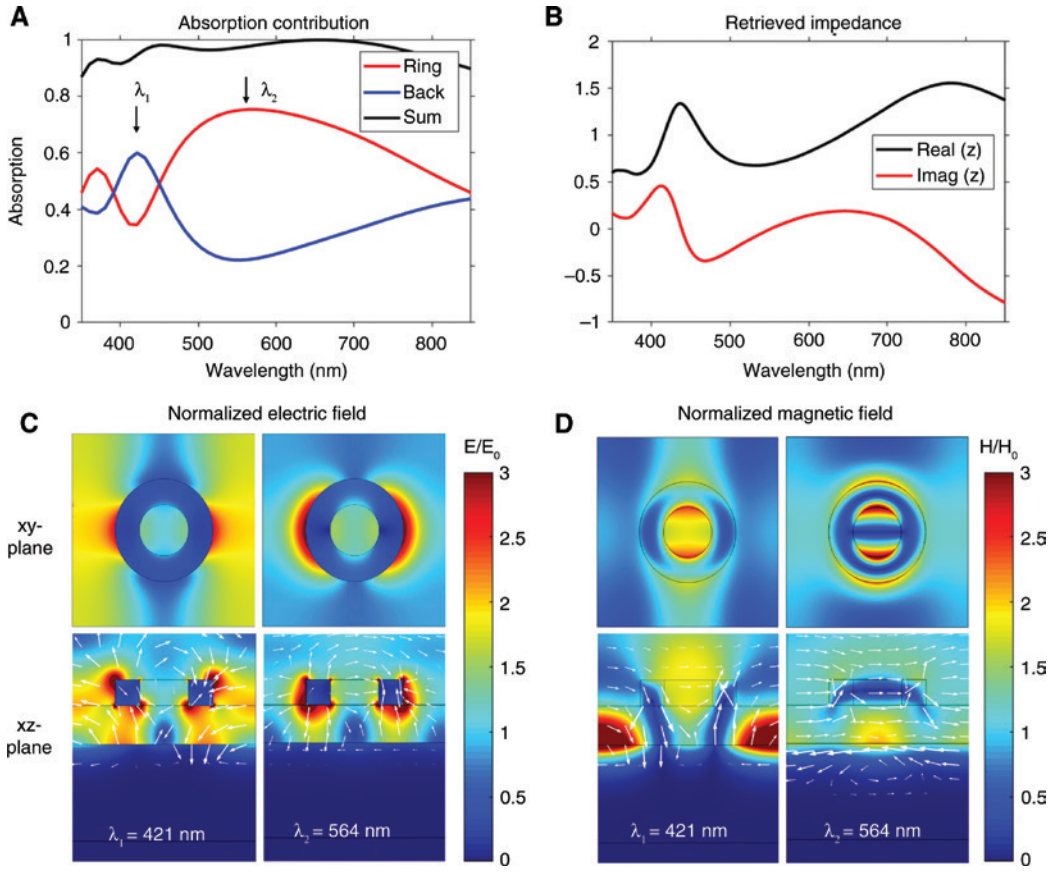

Figure 2: Full-wave electromagnetic simulations for Cr absorbers.
(A) Absorption contribution of each layer. (B) Retrieved homogenous impedance of the device. (C) Calculated normalized electric field (surface plot) and electric field (arrow) along the xy-plane (first row) and xz-plane (second row). (D) Calculated normalized magnetic field (surface plot) and displacement current density (arrow).

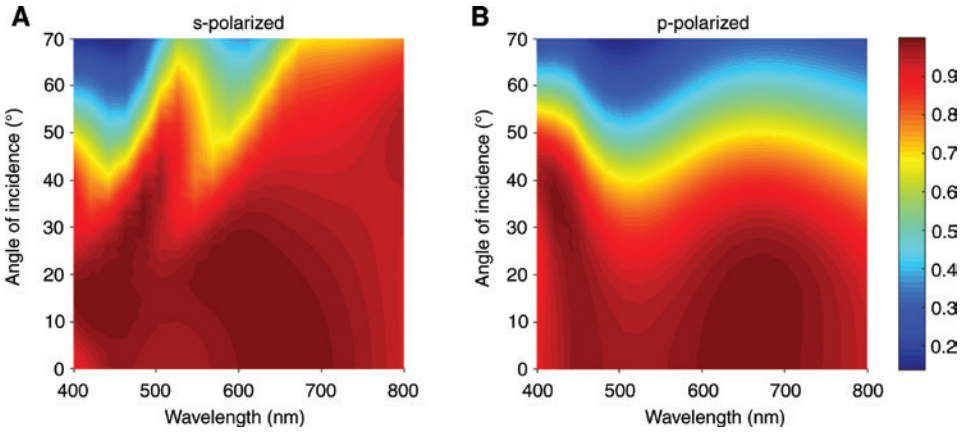

Figure 3: Electromagnetic simulation for absorption change according to incident angle.
Simulated angular dispersions of the absorbance for both polarization: absorbance for incident (A) s-polarized and (B) p-polarized light.

decreased significantly due to the weak confinement of electromagnetic field, especially under p-polarized light. This effect occurs because the resonant natures are very sensitive to the polarization and incident angle. Nevertheless, a broadband absorbance above 80% is maintained up to $\theta_I = 40°$ for both polarizations; this result supports the possibility that our device will have practical applications.

2.2 Thermal stability of the device

To increase thermal and chemical stability, the fabricated Cr metamaterials were coated (Figure 4A) with 4-nm-thick alumina layers that were deposited using atomic layer deposition to prevent the Cr from forming oxides or nitrides after reaction with gases in high-temperature air. Because atomic layer deposition enables almost

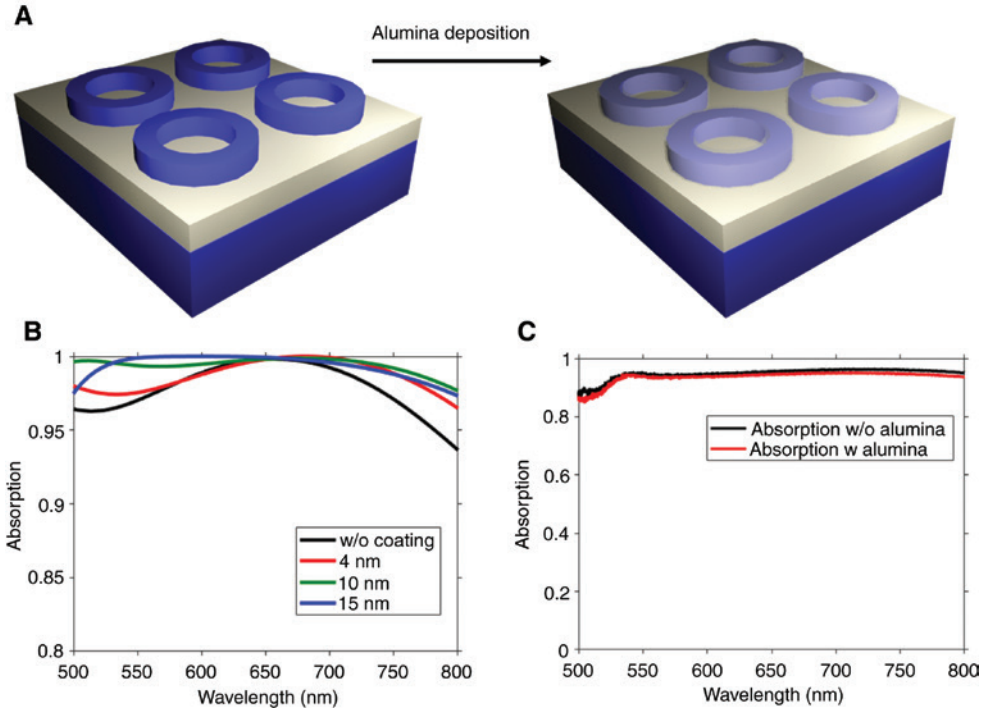

Figure 4: Protection layer coating strategy.
(A) Alumina protection layer coating. Atomic layer deposition method was used and Cr ring structures were perfectly encapsulated.
(B) Absorption contribution of each layer. (C) Absorption spectra of the Cr absorbers with and without 4-nm-thick alumina coat.

100% step coverage, the Cr absorbers that are covered by alumina will be completely sealed.

Using electromagnetic simulations, we checked the influence of alumina thickness on absorption characteristics. The simulation was conducted for alumina layers of 4, 10, and 15 nm. Results confirmed that the absorption characteristics of Cr absorber were maintained up to ~15 nm thickness of alumina (Figure 4B). Alumina thickness of 4 nm did not affect the absorption properties of the device (Figure 4C).

To be useful in high-temperature photonic applications, substances must not undergo chemical reactions (e.g. oxidation and nitridation) in the atmosphere that change their thermal resistance. To investigate the thermal stability of the device, we annealed it in vacuum in a furnace at 600°C for 4 h (Figure 5A). First, we checked the bare Cr absorber (Figure 5B), which is heated at 600°C for 4 h. During the annealing process, all of the structures deformed and expanded when they oxidized (Figure 5E); consequently, the absorber loses its perfect absorption characteristics. However, the 4 nm coat of alumina increased the thermal stability of the absorber (Figure 5C and D), and it retained its shape and absorption characteristics after 600°C annealing (Figure 5F). This alumina can

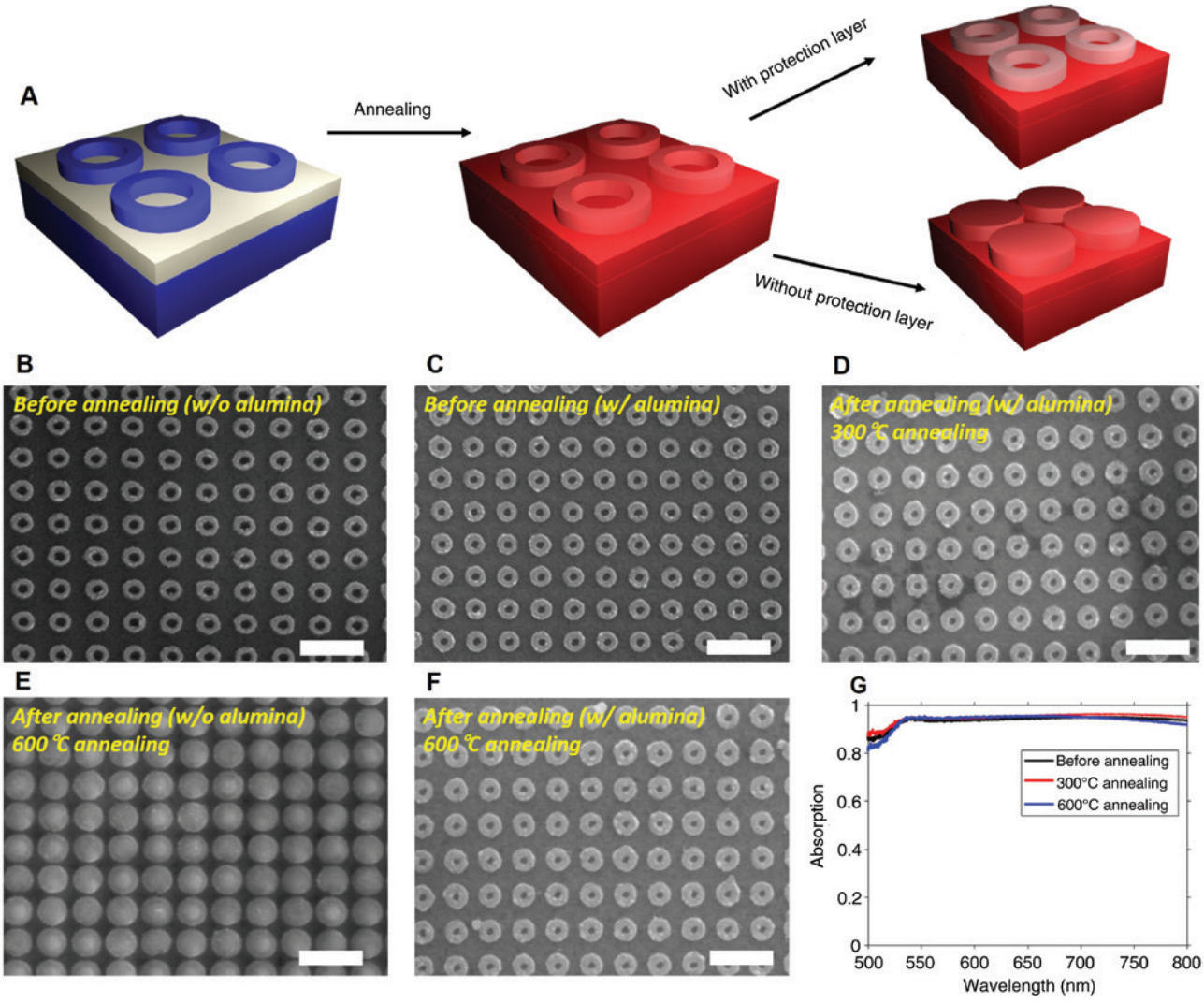

Figure 5: Thermal stability characterizations.
(A) Alumina protection layer coating to improve the heat resistance of the devices. Atomic layer deposition was used and Cr ring structures were perfectly sealed. (B) SEM image of Cr absorber without alumina protective layer before annealing. (C) SEM image of Cr absorber with alumina protection layer before annealing (D) SEM image of Cr absorber with protection layer after annealing at 300°C. (E) SEM image of Cr absorber without protection layer after annealing at 600°C. (F) SEM image of Cr absorber with protection layer after annealing at 600°C. Scale bar, 500 nm. (G) Absorption spectra of Cr absorber coated with 4-nm-thick alumina before and after annealing at 300°C or 600°C.

prevent the oxidation and nitridation of Cr at high temperatures, so it retains its optical properties (Figure 5G).

Our proposed absorber has stable absorption characteristics after annealing at 600°C, but the ring structures actually start to deform at ~600°C. As the Cr ring structures expand during the heating process, the hole inside shrink, and the rings become disks a temperature above 600°C (Figure S1). The simulation result (Figure S2) confirms that as the hole inside decreases in size, the reflectivity increases and the absorption rate decreases. Therefore, Cr nanostructures can maintain a ring shape to a temperature slightly above 600°C (e.g. 650°C), but at higher temperatures the rings become disks, and the function of the absorber is completely lost. The use of a thicker alumina layer and the use of dielectric substrates such as sapphire or silicon nitride may increase the thermal stability.

3 Conclusion

We have proposed an ultra-thin, broadband, and heat-resistant Cr metamaterial absorber that works under visible light with source incidence-angle tolerance of 40°. Ring-shaped structures ensure polarization independence, which is preferable in practical applications. Cr is compatible with fabrication using conventional semiconductor manufacturing processes. It also less expensive than noble metals such as Au and Ag. Under unpolarized light, the Cr absorber can exhibit 95.6% average absorption at $500 \leq \lambda \leq 800$ nm. An alumina protection layer was used to perfectly encapsulate the device to prohibit oxidation and other chemical reactions with the atmosphere. The protected device retain its shape and absorption characteristics even after annealing at 600°C. This Cr metamaterial absorber may enable various high-temperature photonic applications such as STPV and energy harvesting.

4 Experimental section

4.1 Device fabrication

The Cr metamaterial absorbers were fabricated on silicon substrate. First, 150-nm-thick Cr thin film and 60-nm-thick silica layers were deposited by electron beam evaporation at a rate of 0.2 nm/s. Then, on the substrate, the polymethyl methacrylate layer was spin-coated and baked at 180°C for 5 min. A conductive polymer (Showa Denko, Tokyo, Japan, E-spacer 300Z) was spin coated on top of the photoresist layer to prevent charge buildup on the silica layer. Electron beam lithography (ELIONIX, Tokyo, Japan, ELS-7800, 80 kV, 50 pA) was used to scan and expose ring patterns on the photoresist. After exposure, the conductive polymer layer was removed by DI water; then, the exposed photoresist was developed using MIBK:IPA 1:3 solutions. Finally, a 40-nm-thick Cr layer was deposited by electron beam evaporation, and ring-shaped patterns were transferred onto the substrate.

4.2 Optical characterization

Optical measurements (absorption) were performed using FT-IR spectroscopy (Bruker, Billerica, MA, USA, VERTEX 70) with a microscope (Bruker, Billerica, MA, USA, HYPERION 2000) in reflection/transmission mode. Absorptions were calculated from measured reflectance and transmittance.

5 Supplementary material

The supplementary material is available online on the journal's website or from the author.

Acknowledgments: This work was financially supported from the National Research Foundation (NRF) grants (NRF-2018M3D1A1058998, NRF-2017R1E1A1A03070501, NRF-2015R1A5A1037668, and CAMM-2014M3A6B3063708) funded by the Ministry of Science and ICT (MSIT), Republic of Korea. I.K. and S.S. acknowledge the global Ph.D. fellowships (NRF-2016H1A2A1906519 and NRF-2017H1A2A1043322, respectively) from the NRF-MSIT, Republic of Korea. J.R., I.K., and S.S. conceived the concept and initiated the project. I.K. designed and fabricated the device. S.S. performed numerical simulations. I.K. and S.S. conducted the measurements and materials characterization. A.S.R. and M.Q.M provided theoretical advice. I.K., S.S., and J.R. wrote the manuscript. All authors contributed to the discussion and analysis and confirmed the final manuscript. J.R. guided the entire project.

References

[1] Khoaninejad M, Chen WT, Devlin RC, Oh J, Zhu AY, Capasso F. Metalenses at visible wavelengths: diffraction-limited focusing and subwavelength resolution imaging. Science 2016;352: 1190–4.

[2] Chen WT, Zhu AY, Sanjeev V, et al. A broadband achromatic metalens for focusing and imaging in the visible. Nat Nanotechnol 2018;13:220–6.
[3] Wang S, Wu PC, Su VC, et al. A broadband achromatic metalens in the visible. Nat Nanotechnol 2018;13:227–32.
[4] Li Z, Dai Q, Mehmood MQ, et al. Full-space cloud of random points with a scrambling metasurface. Light Sci Appl 2018;7:63.
[5] Yoon G, Lee D, Nam KT, Rho J. Geometric metasurface enabling polarization independent beam splitting. Sci Rep 2018;8:9468.
[6] Ni X, Wong ZJ, Mrejen M, Wang Y, Zhang X. An ultrathin invisibility skin cloak for visible light. Science 2015;349:1310–4.
[7] Zheng G, Mühlenbernd H, Kenney M, Li G, Zentgraf T, Zhang S. Metasurface holograms reaching 80% efficiency. Nat Nanotechnol 2015;10:308–12.
[8] Li Z, Kim I, Zhang L, et al. Dielectric meta-holograms enabled with dual magnetic resonances in visible light. ACS Nano 2017;11:9382–9.
[9] Yoon G, Lee D, Nam KT, Rho J. Pragmatic metasurface hologram at visible wavelength: the balance between diffraction efficiency and fabrication compatibility. ACS Photonics 2018;5:1643–7.
[10] Yoon G, Lee D, Nam KT, Rho J. "Crypto-display" in dual-mode metasurfaces by simultaneous control of phase and spectral responses. ACS Nano 2018;12:6421–8.
[11] Landy NI, Sajuyigbe S, Mock JJ, Smith DR, Padilla WJ. Perfect metamaterial absorber. Phys Rev Lett 2008;100:207402.
[12] Aydin K, Ferry VE, Briggs RM, Atwater HA. Broadband polarization-independent resonant light absorption using ultrathin plasmonic super absorbers. Nat Commun 2011;2:517.
[13] Nguyen DM, Lee D, Rho J. Control of light absorbance using plasmonic grating based perfect absorber at visible and near-infrared wavelengths. Sci Rep 2017;7:2611.
[14] Lee D, Han SY, Jung Y, et al. Experimental demonstration of broadband visible-NIR absorber by plasmonic gratings. Sci Rep 2018;8:12393.
[15] Yoon G, So S, Kim M, Mun J, Ma R, Rho J. Electrically tunable metasurface perfect absorber for infrared frequencies. Nano Converg 2017;4:36.
[16] Liu N, Mesch M, Weiss T, Hentschel M, Giessen H. Infrared perfect absorber and its application as plasmonic sensor. Nano Lett 2010;10:2342–8.
[17] Kim HK, Ling K, Kim K, Lim S. Flexible inkjet-printed metamaterial absorber for coating a cylindrical object. Opt Express 2015;23:5898–906.
[18] Luo M, Shen S, Zhou L, Wu S, Zhou Y, Chen L. Broadband, wide-angle, and polarization-independent metamaterial absorber for the visible regime. Opt Express 2017;25:16715–24.
[19] Chen K, Dao TD, Ishii S, Aono M, Nagao T. Infrared aluminum metamaterial perfect absorbers for plasmonic-enhanced infrared spectroscopy. Adv Funct Mater 2015;25:6637–43.
[20] Narayanaswamy A, Chen G. Surface modes for near field thermophotovoltaics. Appl Phys Lett 2003;82:3544–6.
[21] Nagpal P, Han SE, Stein A, Norris DJ. Efficient low-temperature thermophotovoltaic emitters from metallic photonic crystals. Nano Lett 2008;8:3238–43.
[22] Lenert A, Bierman DM, Nam Y, et al. A nanophotonic solar thermophotovoltaic device. Nat Nanotechnol 2014;9:126–30.
[23] Petrova H, Juste JP, Pastoriza-Santos I, Hartland GV, Liz-Marzán LM, Mulvaney P. On the temperature stability of gold nanorods: comparison between thermal and ultrafast laser-induced heating. Phys Chem Chem Phys 2006;8:814–21.
[24] Rana AS, Mehmood MQ, Jeong H, Kim I, Rho J. Tungsten-based ultrathin absorber for visible regime. Sci Rep 2018;8:2443.
[25] Li Z, Stan L, Czaplewski DA, Yang X, Gao J. Wavelength-selective mid-infrared metamaterial absorbers with multiple tungsten cross resonators. Opt Express 2018;5:5616–31.
[26] Li W, Guler U, Kinsey N, et al. Refractory plasmonics with titanium nitride: broadband metamaterial absorber. Adv Mater 2014;47:7959–65.
[27] Huang Y, Liu L, Pu M, Li X, Ma X, Luo X. A refractory metamaterial absorber for ultra-broadband, omnidirectional and polarization-independent absorption in the UV-NIR spectrum. Nanoscale 2018;10:8298–303.
[28] Bagheri S, Zgrabik CM, Gissibl T, et al. Large-area fabrication of TiN nanoantenna arrays for refractory plasmonics in the mid-infrared by femtosecond direct laser writing and interference lithography. Opt Mater Express 2015;5:2625–33.
[29] Albrecht G, Kaiser S, Giessen H, Hentschel M. Refractory plasmonics without refractory materials. Nano Lett 2017;17:6402–8.
[30] Albrecht G, Ubl M, Kaiser S, Giessen H, Hentschel M. Comprehensive study of plasmonic materials in the visible and infrared: linear, refractory, and nonlinear optical properties. ACS Photonics 2018;5:1058–67.
[31] Jeong HH, Mark AG, Lee TC, et al. Selectable nanopattern arrays for nanolithographic imprint and etch-mask applications. Adv Sci 2015;7:1500016.
[32] Haynes WM. CRC handbook of chemistry and physics. Cleveland, OH, USA, CRC/Taylor and Francis, CRC Press, 2015.
[33] Deng H, Li Z, Stan L, et al. Broadband perfect absorber based on one ultrathin layer of refractory metal. Opt Lett 2015;40:2592–5.
[34] Smith DR, Vier DC, Koschny T, Soukoulis CM. Electromagnetic parameter retrieval from inhomogeneous metamaterials. Phys Rev E 2005;71:036617.

Supplementary Material The online version of this article offers supplementary material (https://doi.org/10.1515/nanoph-2018-0095).